applied sciences

MDPI

Article

Influence of Perfluorooctanoic Acid on Structural, Morphological, and Optical Properties of Hybrid Silica Coatings on Glass Substrates

Violeta Purcar [1], Valentin Rădiţoiu [1], Florentina Monica Raduly [1,*], Alina Rădiţoiu [1], Simona Căprărescu [2], Adriana Nicoleta Frone [1], Raluca Şomoghi [1,3], Mihai Anastasescu [4], Hermine Stroescu [4] and Cristian-Andi Nicolae [1]

[1] National Institute for Research and Development in Chemistry and Petrochemistry—ICECHIM, Splaiul Independentei Street, No. 202, 6th District, 060021 Bucharest, Romania
[2] Faculty of Chemical Engineering and Biotechnologies, Department of Inorganic Chemistry, Physical Chemistry and Electrochemistry, University Politehnica of Bucharest, Ghe. Polizu Street, No. 1-7, 6th District, 011061 Bucharest, Romania
[3] Faculty of Petroleum Refining and Petrochemistry, Petroleum-Gas University of Ploiesti, B-dul Bucureşti, nr. 39, 100680 Ploiesti, Romania
[4] Institute of Physical Chemistry "Ilie Murgulescu" of the Romanian Academy, Splaiul Independentei Street, No. 202, 6th District, 060021 Bucharest, Romania
* Correspondence: monica.raduly@icechim.ro

Abstract: In recent years, various coatings based on fluorinated materials, used in a commercial application, have been created through many preparation routes. However, the techniques utilized to realize these coatings required either expensive and complex equipment, imply multiple manufacturing steps, or are time- or cost-consuming. In this paper, the major target was to develop fluorinated hybrid coatings presenting sustainable hydrophobicity and good transparency simultaneously. The sol–gel method was proposed to obtain these fluorinated hybrid coatings because it does not require expensive equipment, or the existence of stabilizing agents that reduce the storage period, it consumes less energy, and it is easy to implement. The influence of perfluorooctanoic acid, utilized in the sol–gel processing of hybrid silica materials, on the structural, morphological, and optical properties of coatings deposited on glass substrates, was evaluated. Different silane precursors (tetraethyl orthosilicate (TEOS), triethoxymethylsilane (MTES), and trimethoxyhexadecylsilane (HDTMES)) were utilized to synthesize hybrid silica materials. The properties of the obtained materials were characterized by FTIR, UV–Vis, TEM, TGA, AFM, Ellipsometry, and Contact Angle analyses. FTIR spectroscopy shows the formation of a silica network tailored with organofunctional and fluoroalkyl groups. The fluorinated silica coatings presented smooth surfaces and good transparency, with a transmittance of ~90% in the visible range. It was found that the fluorinated silica materials improved the coating's hydrophobicity (~110° in contact angle with water). These fluorinated silica materials can create multifunctional structures with antireflective and hydrophobic coatings for possible optical devices.

Keywords: sol–gel process; fluorinated materials; antireflective coatings; wettability

Citation: Purcar, V.; Rădiţoiu, V.; Raduly, F.M.; Rădiţoiu, A.; Căprărescu, S.; Frone, A.N.; Şomoghi, R.; Anastasescu, M.; Stroescu, H.; Nicolae, C.-A. Influence of Perfluorooctanoic Acid on Structural, Morphological, and Optical Properties of Hybrid Silica Coatings on Glass Substrates. *Appl. Sci.* **2023**, *13*, 1669. https://doi.org/10.3390/app13031669

Academic Editor: Maria Amélia Ramos Loja

Received: 14 December 2022
Revised: 24 January 2023
Accepted: 25 January 2023
Published: 28 January 2023

1. Introduction

Because of their attractive properties, including chemical and thermal stability, non-wetting, high oxygen permeability, and low surface energy, fluorinated materials (e.g., ceramics, polymers, and different types of silicas) have been utilized in many applications (e.g., biomedical [1], pharmaceuticals [2], optoelectronics [3], surface coatings [4], and automotive engineering [5]). Fluorinated derivatives with long chains are extensively used as functional additives or cross-linkers in order to ensure water resistance, together with the chemical and stability properties of the coating. Silica materials are harmonious, with diverse fluorinated functional materials, and can be physically mixed or covalently

attached to a fluorinated component to create composites with special properties [6]. The utilization of silica materials modified with fluorinated organic compounds has attracted great attention due to their significant properties for a large variety of applications (e.g., antimicrobial instruments [7], self-cleaning coatings [8,9], anti-fouling coatings [10], solar cells, and optical devices [11,12]).

Many methods, including chemical vapor deposition [13], physical vapor deposition [14], wet chemical methods [15], hydrothermal methods [16], and the sol–gel process [17], have been adopted to prepare surfaces with micro/nano structures using silane nanoparticles and to create surfaces with water-repellent and self-cleaning properties utilizing hydrophobic materials (e.g., fluoroalkylsilane and silica precursors with different alkyl chain lengths). The chemical vapor deposition technique permits modification of different substrates, but the addition of initiator (e.g., a peroxide) and/or monomers in the vapor phase is required [13]. Physical vapor deposition was used to obtain films with thicknesses of nanometers. The major drawback of this method it is the fact that a high temperature vacuum is required to deposit the film [14]. The sol–gel process is a wet chemical technique and is the most common approach to achieve silica-based materials and fluorinated compositions due to several advantages, such as flexibility, simplicity, low cost, mild reaction conditions, and high-quality materials [18–20]. This method allows for tuning of the structure, morphology, and properties of the resulted materials by changing the reaction conditions [21]. Perfluorooctanoic acid (PFOA) is one of the types of per-fluorinated compounds used to achieve fluorinated materials, because it contains a C-F bond in the molecule with large bond energy. This makes PFOA a chemical with good thermal and chemical stability and excellent hydrophobicity [22].

Several works have reported the development of hybrid materials containing fluorinated compounds, which have special architectures. Employing sol–gel-fluorinated materials in the surface coating resulted in micro- and nanotextured surfaces with excellent properties (e.g., self-cleaning, non-fouling, abrasion-resistant). Guo et al. [23] synthesized fluorinated silica thought the sol–gel method which was able to be applied in applications such as self-cleaning, anti-fouling, and anti-adhesion materials, as well as protection against metal corrosion. It was shown that the achieved material exhibited high transparency (>82%) and good resistance to different media. Yu et al. [24] created a coating film based on fluorinated silica nanoparticles with hydrophobic and anti-aging properties. Startek et al. [25] obtained fluorinated materials by sol–gel method, using fluoroalkyl precursors and silica. The results indicated that longer fluoroalkyl chains can improve the hydrophobicity of the coated surface. The silica nanoparticle-reinforced fluorinated coatings were obtained by Banerjee et al. [26]. The obtained results shown that the fluorosilane concentration was high enough to be encapsulated within the matrix of the coating. Li et al. [27] successfully synthesized fluorinated silica sol through sol–gel processing. The results indicated that the obtained materials used on glass surface presented superhydrophobicity and self-cleaning properties. Huang et al. [28] created nanohybrid silica coating materials by polymerization and the sol–gel process. The performed analysis showed that the nanohybrid film exhibited hydrophobic properties and high transmittance (89–97% in the visible light area). Nimittrakoolchai et al. [29] evaluated the effect of silica nanoparticles coated with the per-fluorinated group on the wettability of the surface. It was revealed that the surfaces presented superhydrophobic properties, which was determined using different liquids (water, ethylene glycol, and seed oil). Shao et al. [30] showed that the mesoporous silica can be modified using fluorinated organosilane. They indicated that the glass surface covered with the prepared materials presented superhydrophobic qualities and excellent thermal stability. Fouhaili et al. obtained fluorinated silica nanoparticles by the sol–gel process. These were deposited on the steel substrates, thus achieving films with superhydrophobic wetting behavior [31]. Saboori et al. [32] synthesized fluorinated nanoparticles through the sol–gel method in order to create surfaces with ultrahydrophobic and ultraoleophobic properties (carbonate and sandstone rock surfaces). Results showed

that the surfaces were stable and presented different levels of wettability as a function of the liquid deposited on the surface.

In the present work, the effect of the fluorinated solution on the structural, morphological, and optical properties of coatings deposited on glass substrates was examined. This fluorinated solution was realized through the dissolution of perfluorooctanoic acid (PFOA) in ethanol, and sol–gel synthesis of hybrid silica materials was utilized to obtain fluorinated coated materials. Silane precursors with different alkyl chain lengths (tetraethyl orthosilicate (TEOS), triethoxymethylsilane (MTES), and trimethoxyhexadecylsilane (HDTMES)) were utilized to synthesize hybrid silica materials. It was demonstrated that the process of obtaining sol–gel fluorinated silica materials does not require the existence of stabilizing agents that reduce the storage period, are easy to implement, and provide smooth layers with uniform thicknesses. The chemical structure, thermal behavior, morphology, wettability, surface roughness, and optical properties of final materials were assessed.

2. Experimental Section

2.1. Materials

Tetraethyl orthosilicate (TEOS), triethoxymethylsilane (MTES), and trimethoxyhexadecylsilane (HDTMES) were acquired from Thermo Fisher Scientific Inc. (Waltham, MA, USA). Perfluorooctanoic acid (PFOA), titanium (IV) isopropoxide (TIP), and maleic anhydride (MA) were obtained from Sigma-Aldrich Co. LLC (Saint Louis, MI, USA). Ethanol (EtOH) and hydrochloric acid solution (HCl 0.1 N) were ordered from PubChem (Bethesda, MD, USA). Analytical-grade chemicals were utilized as received, without further purification.

2.2. Preparation

Hybrid silica materials containing fluorinated solution were synthesized through the acid-catalyzed sol–gel process. In the beginning, the silane precursors (TEOS (3 g), MTES (2.5 g), and/or HDTMES (1.7 g)) were prehydrolyzed in acidic conditions with EtOH (15 g) and HCl 0.1 M (0.5 g) for 15 min, under vigorous magnetic stirring at a temperature of 70 °C ± 2 °C and a speed of 400 rpm. After that, a fluorinated solution (FS, achieved by the dissolving of PFOA (0.03 g) in EtOH (15 g)) was included in the synthesis mixtures, and the stirring was continued for another 45 min. Then, MA (0.06 g) was added to the mixtures, and after its complete dissolution, TIP (0.3 g) was added dropwise. To complete the hydrolysis and condensation reactions, the second part of HCl 0.1 M (1.5 g) was included, and the mixtures were constant stirred for an additional 1 h, maintaining the same temperature (70 °C ± 2 °C). Finally, two stable and homogeneous sol–gel-fluorinated solutions were realized and notated as TEOS/MTES/FS (F1) and TEOS/MTES/HDTMES/FS (F2). The resulting solutions were left to dry at room temperature and then characterized as powdered materials (obtained by placing the solution in plastic vials and analyzed after solvent evaporation) and as fluorinated hybrid coatings (achieved by deposition of materials only on one side of the glass substrates using a manual film applicator (Multicator 411, Erichsen, Minneapolis, MN, USA)). Before being used, the glass substrates were washed with a detergent and deionized water for 30 min in an ultrasonic bath, followed by cleaning with acetone, ethyl alcohol, and deionized water. The washing and cleaning process was repeated three times. Afterwards, the glass substrates were positioned in a desiccator and dried for 24 h in a vacuum to remove possible reactants and contaminants, as well as to obtain high-quality coatings. The schematic illustration of the synthesis procedure to achieve fluorinated silica materials as powdered materials and as fluorinated hybrid coatings is shown in Figure 1.

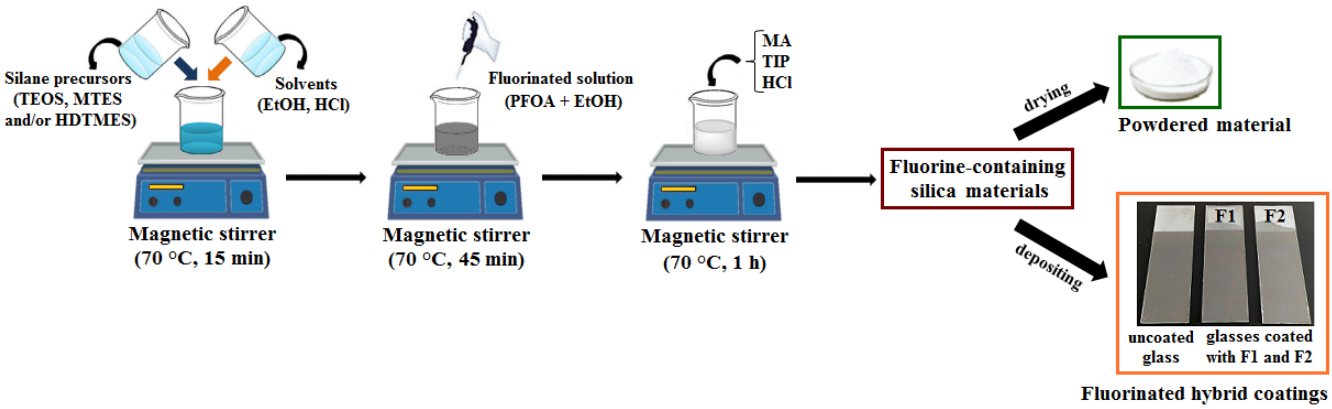

Figure 1. Schematic illustration of synthesis procedure to obtain fluorinated silica materials as powdered materials and as fluorinated hybrid coatings.

2.3. Methods

FTIR spectra of fluorinated silica materials were recorded on a Fourier Transformed Infrared spectrometer (FTIR, model FT–IR 6300, Jasco Int. Co. Ltd., San Francisco, CA, USA) equipped with a 3-inch sphere (model PIKE Mid-IR IntegratIR, Madison, WI, USA), and evaluated from 500 to 5000–500 cm^{-1} range.

Thermogravimetric analysis (TGA) was performed on a TA TGA Q500 IR instrument (TA Instruments, Pittsburgh, PA, USA) working in the 30–750 °C range, under a nitrogen atmosphere, at a heating rate of 10 °C/min. Powdered materials (8–10 mg) were analyzed using alumina crucibles.

The fluorinated silica materials were analyzed through Transmission Electron Microscopy (TEM, model TECNAI F20 G^2 TWIN Cryo–TEM, FEI Company, Hillsboro, OR, USA) at 200 kV accelerating voltage.

Atomic Force Microscopy (AFM) measurements were performed with a microscope produced by Park Systems (XE–100 model) working in non-contact mode. The microscope is able to obtain accurate images due to its configuration, namely its decoupled XY/Z and flexure-guided cross-talk eliminated scanners. In all AFM experiments, sharp tips with less than a 10 nm radius of curvature, ~125 µm length, ~30 µm width, ~42 N/m force constant, and ~330 kHz resonance frequency (NCHR, Nanosensors™) were used. The AFM images were processed with the XEI program (v 1.8.0—Park Systems) for thermal tilt correction and roughness assessment. The root-mean-squared roughness (R_q) is the standard deviation of the height value in the image, and the peak-to-valley parameter (R_{pv}) indicates the height difference between the minimum and the maximum. The AFM images are shown in "enhanced color"™ view mode, accompanied by representative line scans which show the surface z-axis in detail.

The spectroscopic ellipsometry (SE) measurements were achieved on a VASE ellipsometer (J.A. Woollam. Co., Lincoln, NE, USA) at a 65° angle of incidence, in the range of 400–800 nm, with a 10 nm step. The film thickness, roughness, and fit error (mean square error—MSE) were achieved through fitting the experimental spectroscopic ellipsometry (SE) spectra with a model based on the references within the commercial WVASE32™ software (version 3.920). Transmittance spectra of fluorinated hybrid coatings were measured by SE in the 250–800 nm wavelength range.

Diffuse reflectance spectra of fluorinated hybrid coatings were carried out by an ultraviolet–visible (UV–Vis) spectrophotometer (model UV-VIS-NIR-Jasco V–570, JASCO Int. Co. Ltd., San Francisco, CA, USA) equipped with a large integrating sphere (model ILN-472, JASCO Int. Co. Ltd., San Francisco, CA, USA); they were recorded in the range from 780 to 380 nm. Each hybrid coating was analyzed three times (standard deviation ± 0.2%).

The water contact angles of the coatings were measured using a tensiometer (model CAM 200, KSV Instruments Ltd., Monroe, WI, USA) connected to a high-resolution camera (Basler A602f, Ahrensburg, Germany). The results of the static contact angle were the mean

value of 20 single measurements. Water droplets (~6 µL) were placed carefully in various zones of the coatings.

3. Results and Discussion

3.1. FTIR Spectoscopy

FTIR spectra of the fluorinated silica materials, obtained as powdered materials, are shown in Figure 2. The bands at ~940 and ~1050 cm^{-1}, which appear in both spectra of samples F1 and F2, may be assigned to Si–O–Si bonds (asymmetric stretching vibration or bending vibrations) [33]. The bands observed at ~1630 and ~3420 cm^{-1} are attributed to OH bending and stretching vibrations, respectively [34]. The peak that appears at ~1272 cm^{-1} corresponds to the stretching vibrations of Si–CH_3 bonds [35]. The band localized at ~1410 cm^{-1} is related to C–H bonds (asymmetric deformation) and –CH_2– groups (scissors vibration) [36]. Moreover, in both samples, a peak at ~775 cm^{-1} was detected that belongs to C–H bonds (out-of-plane vibration) [37]. The peak that appeared at ~1380 cm^{-1} is assigned to C–H asymmetric stretching in –CH_3 aliphatic group [25]. In addition, the characteristic band at 658 cm^{-1} is attributed to the characteristic of –CF_2 [38]. Thus, it was demonstrated that the organic alkyl chains derived from silane precursors are covalently attached to the PFOA.

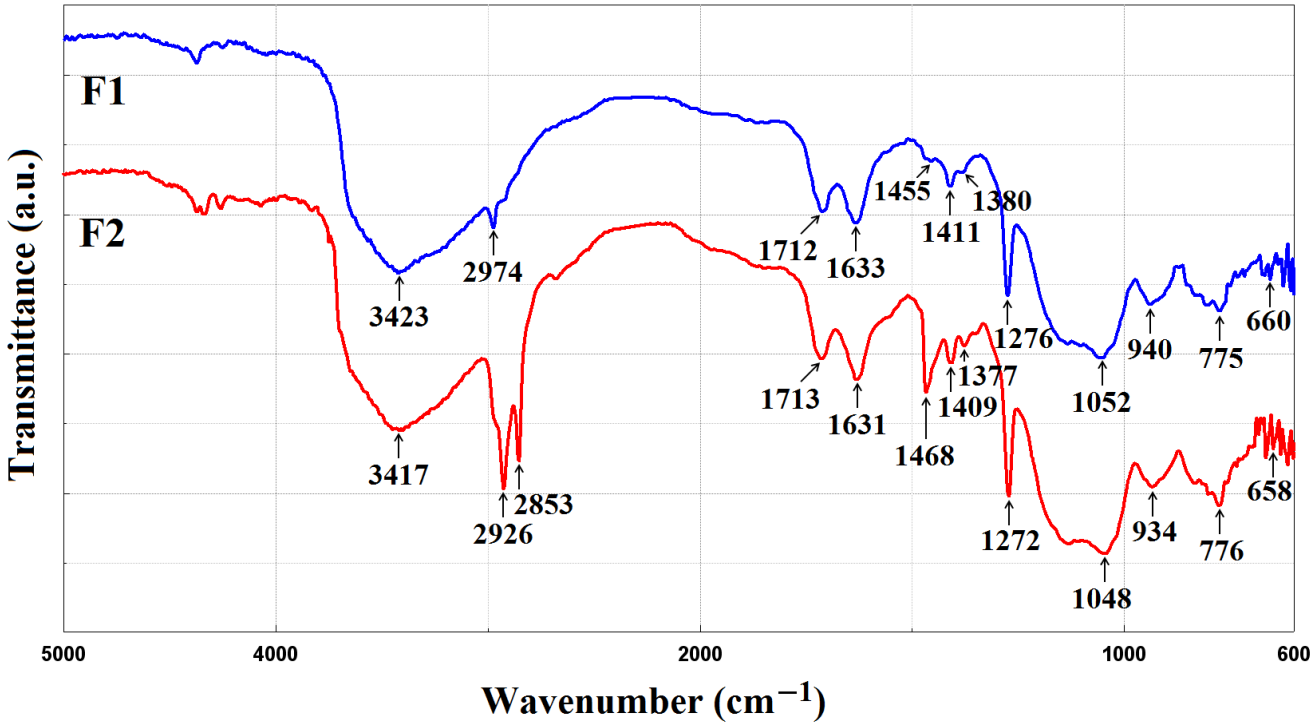

Figure 2. FTIR spectra of fluorinated silica materials (as powders): TEOS/MTES/FS (F1) and TEOS/MTES/HDTMES/FS (F2).

In the FTIR spectrum of sample F1, a peak at 2974 cm^{-1} was detected which corresponds to the stretching vibration of the –CH_3 groups [39]. The characteristic band of –CH_2 (scissoring vibration) is present at 1455 cm^{-1} [40]. In the FTIR spectrum of sample F2, other peaks were observed in the range of 2925–2853 cm^{-1} and are attributed to C–H bonds originating from stretching vibrations of the –CH_3 and –CH_2– groups [41,42]. The intensity of these peaks was found to be increased as compared to that of those noted for sample F1. This result is consistent with the assumption that the incorporation of HDTMES in the solution leads to the replacement of surface −OH groups by more −CH_3 groups [37]. Another peak at 1468 cm^{-1} was detected and is assigned to the aliphatic CH– groups originating from the organic groups (scissoring vibration) [43].

By analyzing Figure 2, it can be concluded that organo-silicate networks were created that contained siloxane groups, alkyl chains, and fluoroalkyl chains derived from the silane precursors and from perfluorooctanoic acid (see Scheme 1).

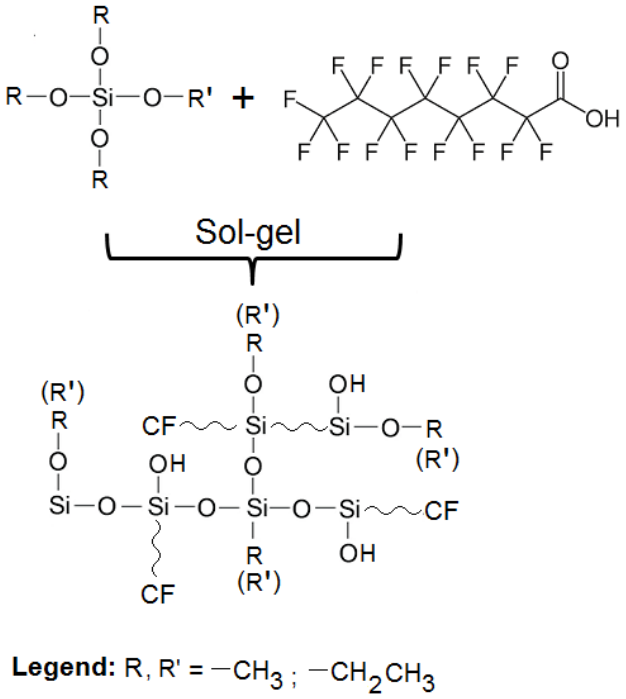

Scheme 1. Probable reaction mechanism than can occur between silane precursors and perfluorooctanoic acid.

3.2. TGA Analysis

Figure 3 reveals the TGA analysis of the fluorinated silica materials. The decomposition temperature (T_{max}) and the weight loss (Wt. loss %) of these materials are presented in Table 1. From this figure, it can be noticed that the thermal decomposition curves of the fluorinated silica materials through the TGA are divided into three thermal events. The first zone, occurring at a temperature of 30–100 °C, is attributed to dehydration of the water and of residual organic solvent and exhibits a weight loss of about 1–4%. The second zone is illustrated at the 100–240 °C range and displays a weight loss of approximately 3–8%. The intermediate temperature peak is frequently assigned to the condensation of non-hydrolyzed groups (≡Si–OH, ≡Si–OCH_2CH_3) arising from the used silane precursors and from species derived from molecules physically entrapped inside the silica matrix [44]. The third zone, occurring at the 240–750 °C, range exhibits a weight loss of about 4–27%. The result shows that the sample synthesized with TEOS/MTES/FS (F1) has slightly lower slopes than the other sample prepared with TEOS/MTES/HDTMES/FS (F2), which means that the long alkyl chains slightly increased the stability of the prepared material. In previous data published in the literature [45], it was indicated that the values of the initial degradation temperature of the fluorinated composites without and with silica were 307 °C and 315 °C, respectively. This change was attributed to the presence of silica in the composites, and to formation of the Si–O–Si bonds. It was also shown that the oxidation of alkyl groups (responsible for the hydrophobic behavior of silica material) can occur at high temperatures [46].

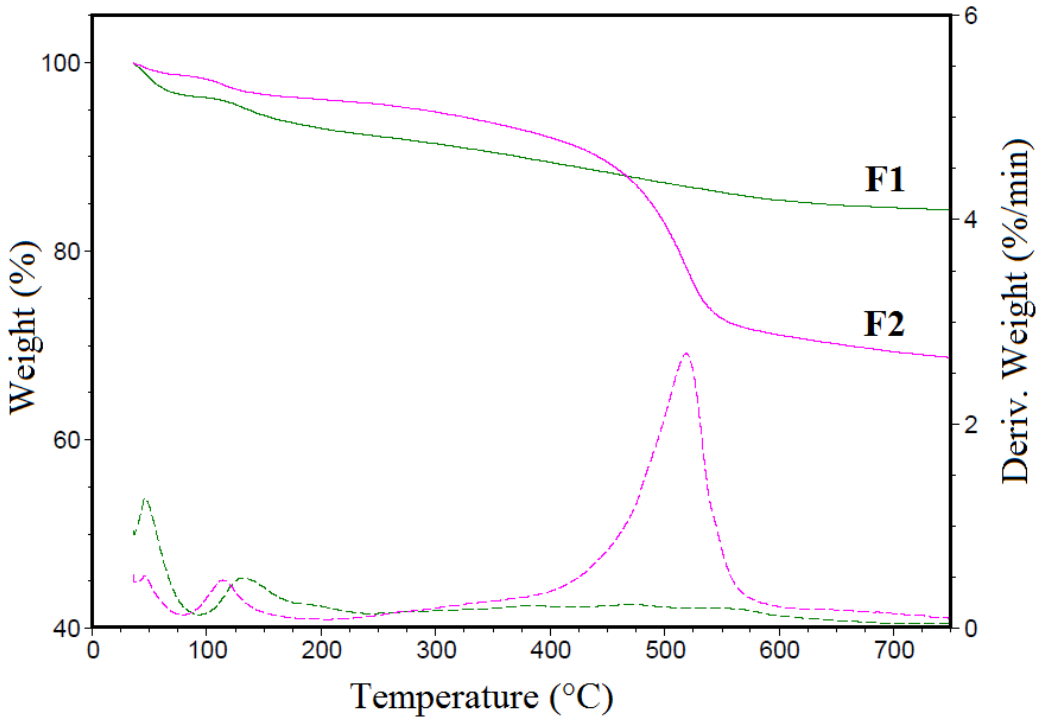

Figure 3. TGA curves of the fluorinated silica materials (as powdered materials): TEOS/MTES/FS (F1) and TEOS/MTES/HDTMES/FS (F2).

Table 1. The maximum decomposition temperature (T_{max}) and weight loss (Wt. loss %) of the fluorinated silica materials, obtained as powdered materials (30–750 °C range).

Sample	30–100 °C	100–240 °C		240–750 °C		Residue at 750 °C
	Wt. Loss %	Wt. Loss %	T_{max} [1] °C	Wt. Loss %	T_{max} °C	N_2 %
F1	3.64	7.94	131.6	4.04	470.7	84.37
F2	1.38	2.59	114.1	27.31	518.8	68.72

[1] T_{max} (°C) = $T(d\alpha/dt)_{max}$.

3.3. TEM Analysis

The morphology of the fluorinated silica materials (powdered samples) was carried out by TEM microscopy (see Figure 4). The TEM images show that the fluorinated silica materials were cross-linked by the covalently bonded Si–O–Si structures. In both samples, no phase separations were observed, and it can thus be found that reactions occurred successfully by hydrolysis as well as condensation of silane precursors and perfluorooctanoic acid. In previous reports, it was shown that the stacked organization of the alkyl chains may be due to the maximized van der Waals interactions of the chains [47]. It was also demonstrated that the morphology of the silica material can be changed as a function of the functionalization of the silica surface with alkyl groups arising from silane precursors [48].

3.4. AFM Analysis

Figure 5 displays the bi-dimensional AFM topographic images of samples F1 and F2 deposited on glass substrates, at a scale of 4 μm × 8 μm. AFM images were scanned firstly over larger scales, in order to prove that the films were adherent to the substrate used and to check the corrugation of the surfaces. Sample F1 exhibited random "bumps" which were a few nm in height and 100–300 nm in diameter (see Figure 5a and the red line in Figure 5c), and, additionally, a few pits no deeper than 10 nm (see the green line in Figure 5c). Sample F2 showed some wavy-like parcels (as seen in the red line from

Figure 5d) and some deposits of materials (see the right down corner), but in between these defects, the surface was uniform (see the green line in Figure 5d).

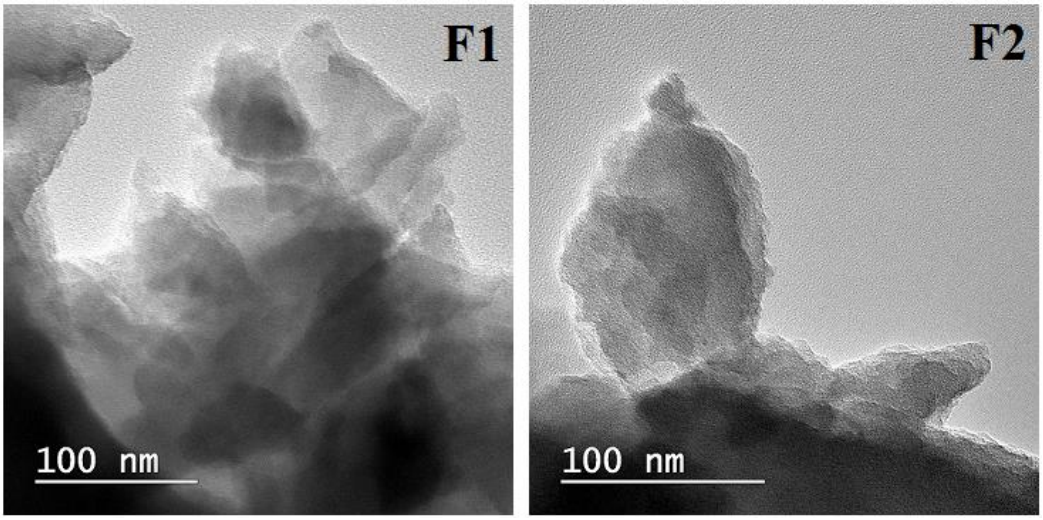

Figure 4. The TEM images of fluorinated silica materials (powdered samples): TEOS/MTES/FS (F1), and TEOS/MTES/HDTMES/FS (F2).

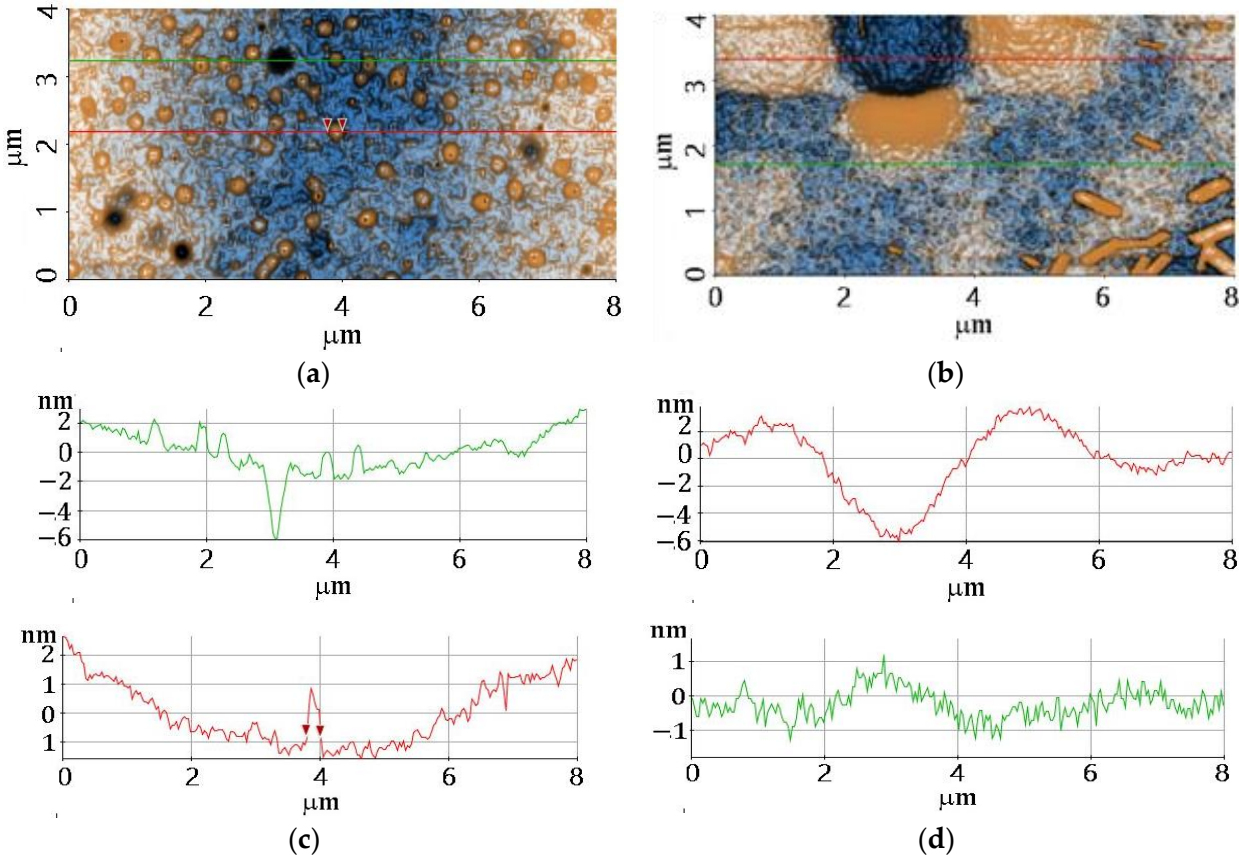

Figure 5. 2D AFM images (enhanced contrast) scanned over 4 μm × 8 μm, together with two representative line scans collected along the X-axis (the positions are indicated in each AFM figure) for fluorinated hybrid coatings: sample F1 (**a**,**c**) and sample F2 (**b**,**d**).

Figure 6 exhibits the morphology of samples F1 and F2, deposited on glass substrates. It was obtained from bi-dimensional AFM topographic images, scanned over an area of 2 μm × 2 μm.

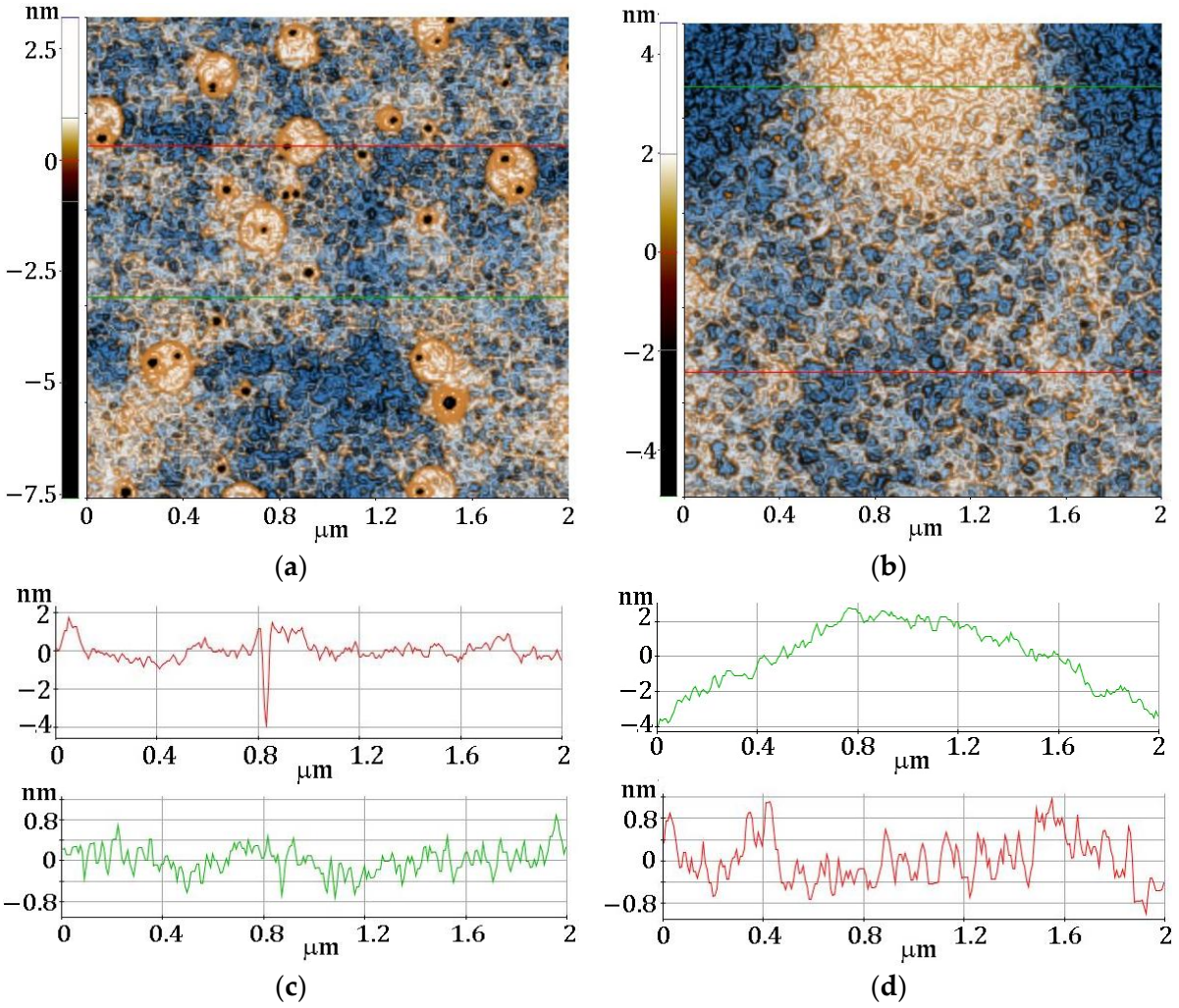

Figure 6. 2D AFM images (enhanced contrast) scanned over 2 μm × 2 μm together with two representative line scans collected along the green and red lines (the positions are indicated in each AFM figure) for fluorinated hybrid coatings: sample F1 (**a**,**c**) and sample F2 (**b**,**d**).

As can be observed from Figure 6a,b, on smaller scales of 2 μm × 2 μm, both samples were relatively smooth, as observed from the arbitrary line-scans collected by Figure 6c,d in different areas. While sample F1 (Figure 6a) exhibited randomly distributed small pores, visible as dark spots a few nm deep (see the red line in Figure 6c), sample F2 (Figure 6b) presented level differences in the z-axis no higher than 6 nm (see the green line in Figure 6d). Figure 7 shows the root-mean-square roughness of the F1 and F2 coatings in comparison with the uncoated glass substrate. It can be seen that at low scales (2 μm × 2 μm), both F1 and F2 coatings were smooth, as their RMS roughness's did not exceed 1.2 nm, while at larger scales (4 μm × 8 μm), sample F2 became more corrugated due to some protuberances formed during film deposition. The roughness is in line with the values of water contact angles, but it is also influenced by the chemical differences between the fluorinated silica-based coatings.

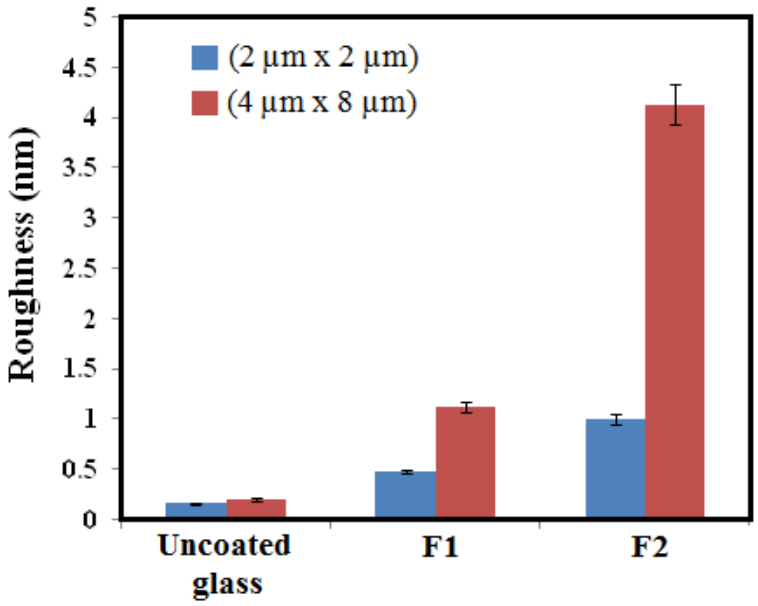

Figure 7. Root-mean-square roughness for the uncoated glass and the fluorinated hybrid coatings (TEOS/MTES/FS (F1) and TEOS/MTES/HDTMES/FS (F2)), at the scales of 2 µm × 2 µm, and 4 µm × 8 µm.

The film thickness (d_{film}), roughness, and fit error (mean square error—MSE) were achieved through fitting the experimental spectroscopic ellipsometry (SE) spectra, and their values are presented in Table 2. The roughness increased with the sample's thickness, although the absolute values were very low, revealing a smooth surface, which was also underlined by AFM measurements.

Table 2. Thickness (d_{film}), roughness, and fit error (MSE).

Sample	d_{film} (nm)	Roughness (nm)	MSE
F1	1052	0.93	1.804
F2	1570	2.34	1.468

3.5. Optical Analysis

The transmittance spectra of the fluorinated hybrid coatings (achieved through the deposition of fluorinated silica materials on glass substrates) were measured by spectroscopic ellipsometry (SE) in the 250–800 nm wavelength range. The spectra are presented in Figure 8. All samples presented a good transmission of more than 85% in the visible spectral range. An interesting small increase was observed in the transmission of the F1 sample in comparison with the uncoated glass substrate, but a decrease in the transmission was also observed for sample F2, which could be correlated with the increase in F2's sample thickness leading to an increase in the absorption. It can also be seen that the F1 spectrum starts at 85% transmittance, while the F2 spectrum starts at 65% transmittance, indicating that the addition of more $-CH_3$ groups from HDTMES effectively utilized more light. In previous reports, it has been shown that films of lower thicknesses always have a lower optical gap [49].

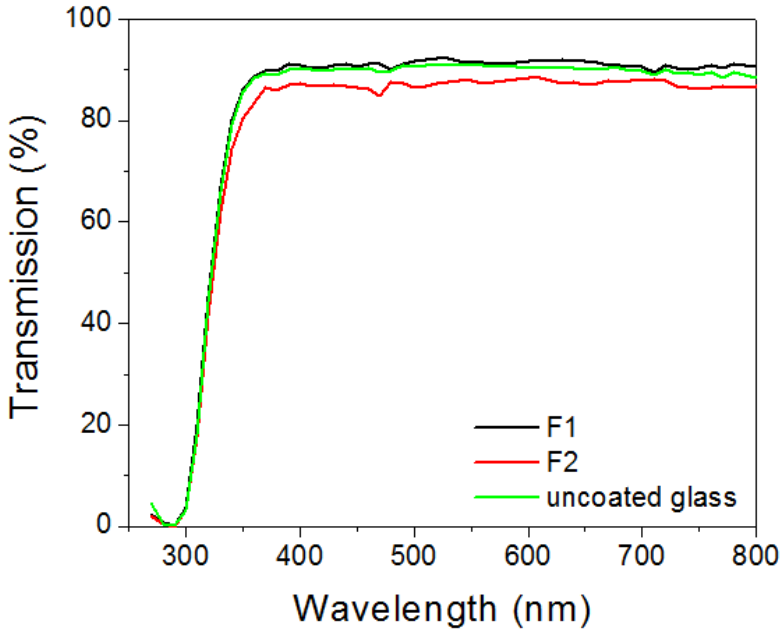

Figure 8. Transmittance spectra of the uncoated glass and the fluorinated hybrid coatings (TEOS/MTES/FS (F1) and TEOS/MTES/HDTMES/FS (F2)).

Figure 9 reveals the diffuse reflectance spectra of fluorinated hybrid coatings, recorded in the range of 380–780 nm.

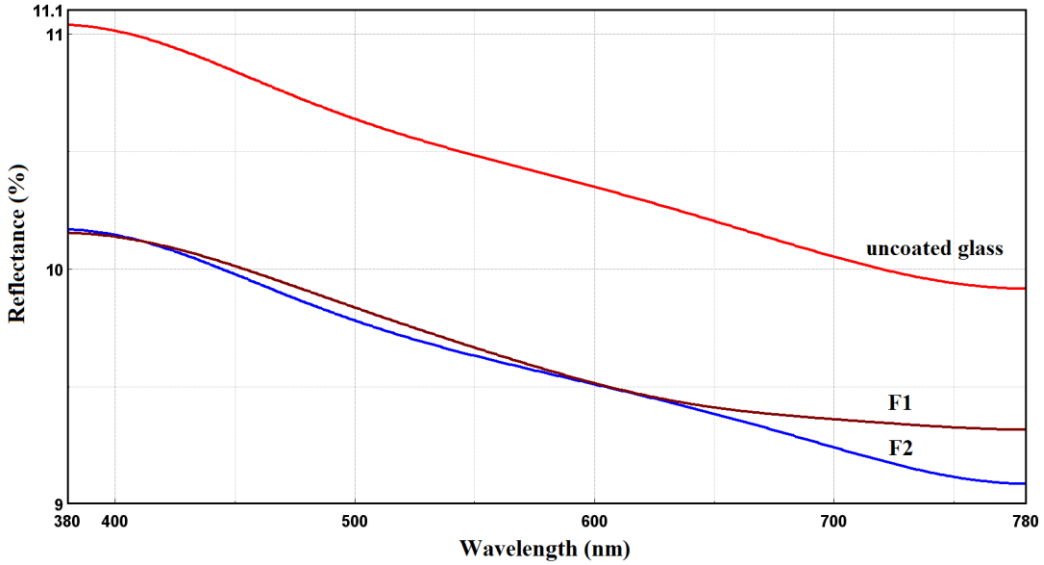

Figure 9. Diffuse reflectance spectra of the uncoated glass and the fluorinated hybrid coatings (TEOS/MTES/FS (F1) and TEOS/MTES/HDTMES/FS (F2)).

As can be seen in Figure 9, the diffuse reflectance spectrum of uncoated glass was found to be ~10.5% (l = 550 nm). In the case of glass substrates coated with the fluorinated silica materials (samples F1 and F2), the reflectance was ~9.7%. Both fluorinated hybrid coatings presented lower reflectance than the uncoated glass. It can also be observed that the reflectance of the fluorinated hybrid coatings decreases as the wavelength range increases. From the obtained results, it can be concluded that the silanization of the glass substrates with fluorinated silica materials is helpful in lowering reflectivity.

In previous papers, it has been shown that to produce electricity (for example, in photovoltaic systems), coatings with antireflective effects play a significant role in reducing losses, owing to the reflection of sunlight [50].

3.6. Contact Angle Measurements

The analysis of the water contact angle of the surfaces is an easy method for detecting surface changes at the monolayer level. In previous papers, it has been shown that wetting behavior is influenced by the nature and length of the pendent chain [51], as well as the surface group's concentration [36].

The values of the water contact angles and profiles of the water drops on the uncoated glass substrate and the glass substrates coated with fluorinated silica materials (samples F1 and F2) are shown in Figure 10. According to this figure, it can be observed that the wetting behavior of coatings depends on the fluorinated silica materials which were deposited onto the glass substrates. Both samples F1 and F2 developed a hydrophobic property ($92 \pm 1.3°$, and $110 \pm 1.2°$, respectively) in comparison with uncoated glass substrate ($35 \pm 1.6°$). In the case of fluorinated hybrid coatings, some of the silanol groups on the film surface were replaced by alkyl groups (methyl, hexadecyl), and this phenomenon led to a modification of the surface activity.

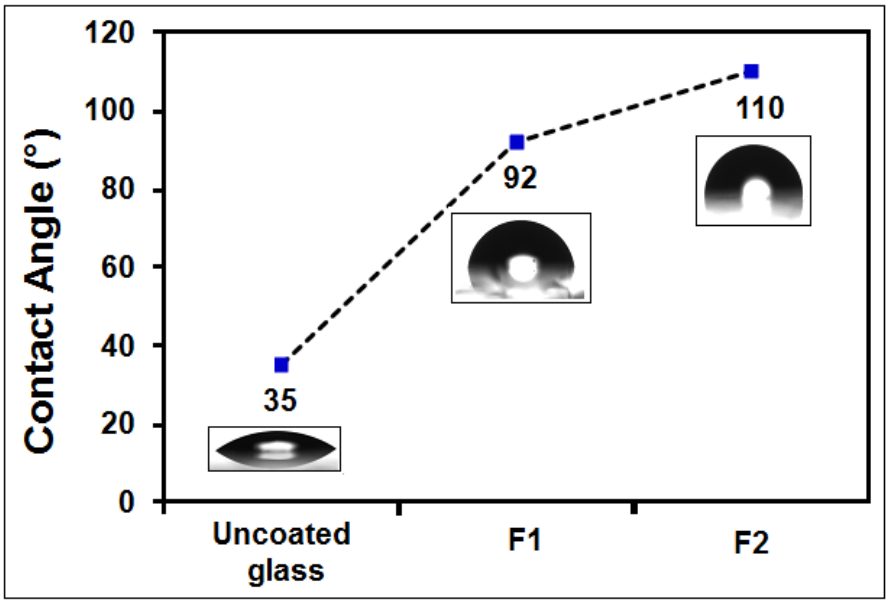

Figure 10. Values of the water contact angles and profiles of the water drops on the uncoated glass and the fluorinated hybrid coatings (TEOS/MTES/FS (F1) and TEOS/MTES/HDTMES/FS (F2)).

The increase in the water contact angle values can be attributed to the length of the functional group, following the order of MTES < HDTMES. It has been reported that the coating exhibits a hydrophilic character when the interaction forces between the water and the substrate are almost equal to the cohesive forces of the bulk water. In this case, the water does not drain cleanly from the substrate. The decrease in the contact angle may be due to unstable siloxane groups (Si–O–Si) or the presence of free silanol groups (Si–OH). These groups create polar and reactive surfaces, conferring interaction with water molecules that were physically adsorbed through the hydrogen bonds [52]. In previous reports, it has been demonstrated that the water contact angle increase could be associated with to a large amount of air entrapment between the silica material, forming a composite microstructure of the solid film and the air that reduces the effective contact area of water from the surface [53].

4. Conclusions

In this paper, the fluorinated silica materials were realized via an acid-catalyzed sol–gel process using different silane precursors (TEOS, MTES, and/or HDTMES) and fluorinated solution. The transparent and antireflective fluorinated hybrid coatings were achieved by the deposition of these materials onto glass substrates. The presented results indicated the relationship between the silane precursors (utilized in the synthesis of hybrid silica materials) and the final properties of the created coatings. The chemical structure, thermal behavior, morphology, wettability, and surface properties of the resulted materials were evaluated by FTIR, UV–Vis, TEM, TGA, AFM, ellipsometry analysis, and water contact angle measurements. The FTIR spectra showed that organo-silicate networks were formed, which included siloxane groups, alkyl chains, and fluoroalkyl chains derived from the silane precursors and from the fluorinated solution. TEM images demonstrated that the fluorinated silica materials had been cross-linked by the covalently bonded Si–O–Si structures. Optical analysis revealed that the fluorinated hybrid coatings presented lower reflectance (~9.7%, at 550 nm) than the uncoated glass substrate, as well as good transparency, with a transmittance of ~90% in the visible range. Water contact angle analysis indicated that the fluorinated hybrid coatings developed hydrophobic properties (~110°). Although there are fluorinated reactive silanes that are commercially available and can be utilized with the sol–gel method, they are, in a great measure, limited to linear per-fluorinated carbon chains, which diminishes the chemical variation and the scope of the fluorinated materials. The rational structure engineering and the mechanism study are the essential scientific issues to be discussed for the future development of fluorinated materials, which will present excellent performance in large-scale applications (e.g., electronics, energy storage devices, and protective coatings).

Author Contributions: Conceptualization, V.P. and V.R.; methodology, V.P. and V.R.; formal analysis, F.M.R., A.R., A.N.F., R.Ş., M.A., H.S. and C.-A.N.; investigation, F.M.R., A.R. and S.C.; data curation, A.N.F., R.Ş., M.A., H.S. and C.-A.N.; writing—original draft preparation, V.P. and S.C.; writing—review and editing, V.P. and S.C. All authors have read and agreed to the published version of the manuscript.

Funding: This research was funded by the INCDCP ICECHIM Bucharest 2019–2022 Core Program PN. 19.23–Chem-Ergent, Project No.19.23.03.01.

Institutional Review Board Statement: Not applicable.

Informed Consent Statement: Not applicable.

Data Availability Statement: The data are not publicly available due to their containing information that could compromise the privacy of research participants.

Conflicts of Interest: The authors declare no conflict of interest.

References

1. Cardoso, V.F.; Correia, D.M.; Ribeiro, C.; Fernandes, M.M.; Lanceros-Méndez, S. Fluorinated Polymers as Smart Materials for Advanced Biomedical Applications. *Polymers* **2018**, *10*, 161. [CrossRef] [PubMed]
2. Haranahalli, K.; Honda, T.; Ojima, I. Recent progress in the strategic incorporation of fluorine into medicinally active compounds. *J. Fluor. Chem.* **2019**, *217*, 29–40. [CrossRef]
3. Martinelli, C.; Farinola, G.M.; Pinto, V.; Cardone, A. Synthetic Aspects and Electro-Optical Properties of Fluorinated Arylenevinylenes for Luminescence and Photovoltaics. *Materials* **2013**, *6*, 1205–1236. [CrossRef] [PubMed]
4. El-Maiss, J.; Darmanin, T.; Guittard, F. Branched versus linear perfluorocarbon chains in the formation of superhydrophobic electrodeposited films with low bioaccumulative potential. *J. Mater. Sci.* **2014**, *49*, 7760–7769. [CrossRef]
5. Gardiner, J. Fluoropolymers: Origin, Production, and Industrial and Commercial Applications. *Aust. J. Chem.* **2015**, *68*, 13–22. [CrossRef]
6. Iacono, S.T.; Jennings, A.R. Recent Studies on Fluorinated Silica Nanometer-Sized Particles. *Nanomaterials* **2019**, *9*, 684. [CrossRef] [PubMed]
7. Storm, W.L.; Youn, J.; Reighard, K.P.; Worley, B.V.; Lodaya, H.M.; Shin, J.H.; Schoenfisch, M.H. Superhydrophobic nitric oxide-releasing xerogels. *Acta Biomater.* **2014**, *10*, 3442–3448. [CrossRef]

8. Huang, Y.; Yi, S.; Lv, Z.; Huang, C. Facile fabrication of superhydrophobic coatings based on two silica sols. *Colloid Polym. Sci.* **2016**, *294*, 1503–1509. [CrossRef]
9. Ray, S.S.; Lee, H.K.; Huyen, D.T.T.; Park, Y.-I.; Park, H.; Nam, S.-E.; Kim, I.-C.; Kwon, Y.-N. Fluorine-free anti-droplet surface modification by hexadecyltrimethoxysilane-modified silica nanoparticles-coated carbon nanofibers for self-cleaning applications. *Prog. Org. Coatings* **2021**, *153*, 106165. [CrossRef]
10. Oldani, V.; del Negro, R.; Bianchi, C.L.; Suriano, R.; Turri, S.; Pirola, C.; Sacchi, B. Surface properties and anti-fouling assessment of coatings obtained from perfluoropolyethers and ceramic oxides nanopowders deposited on stainless steel. *J. Fluor. Chem.* **2015**, *180*, 7–14. [CrossRef]
11. Jennings, A.R.; Iacono, S.T. Progress in fluorinated organically modified silicas. *Polym. Int.* **2016**, *65*, 6–10. [CrossRef]
12. Fujihara, S. Sol-Gel Processing of Fluoride and Oxyfluoride Materials. In *Handbook of Sol-Gel Science and Technology*; Klein, L., Aparicio, M., Jitianu, A., Eds.; Springer: Cham, Switzerland, 2018. [CrossRef]
13. Vilaró, I.; Yagüe, J.L.; Borrós, S. Superhydrophobic Copper Surfaces with Anticorrosion Properties Fabricated by Solventless CVD Methods. *ACS Appl. Mater. Interfaces* **2017**, *9*, 1057–1065. [CrossRef] [PubMed]
14. Dobrzański, L.A.; Gołombek, K.; Lukaszkowicz, K. Physical Vapor Deposition in Manufacturing. In *Handbook of Manufacturing Engineering and Technology*; Nee, A., Ed.; Springer: London, UK, 2013. [CrossRef]
15. Vasconcelos, H.C. Optical Waveguides Based on Sol-Gel Coatings. In *Electromagnetic Propagation and Waveguides in Photonics and Microwave Engineering*; Steglich, P., Ed.; IntechOpen: London, UK, 2020; pp. 1–18. [CrossRef]
16. Raimondo, M.; Veronesi, F.; Boveri, G.; Guarini, G.; Motta, A.; Zanoni, R. Superhydrophobic properties induced by sol-gel routes on copper surfaces. *Appl. Surf. Sci.* **2017**, *422*, 1022–1029. [CrossRef]
17. Li, Y.; Men, X.; Zhu, X.; Ge, B.; Chu, F.; Zhang, Z. One-step spraying to fabricate nonfluorinated superhydrophobic coatings with high transparency. *J. Mater. Sci.* **2016**, *51*, 2411–2419. [CrossRef]
18. Navas, D.; Fuentes, S.; Castro-Alvarez, A.; Chavez-Angel, E. Review on Sol-Gel Synthesis of Perovskite and Oxide Nanomaterials. *Gels* **2021**, *7*, 275. [CrossRef] [PubMed]
19. Bokov, D.; Jalil, A.T.; Chupradit, S.; Suksatan, W.; Ansari, M.J.; Shewael, I.H.; Valiev, G.H.; Kianfar, E. Nanomaterial by Sol-Gel Method: Synthesis and Application. *Adv. Mater. Sci. Eng.* **2021**, *2021*, 5102014. [CrossRef]
20. Seck, S.; Magana, S.; Prébé, A.; Niepceron, F.; Bounor-Legaré, V.; Bigarré, J.; Buvat, P.; Gérard, J. PVDF-HFP/silica-SH nanocomposite synthesis for PEMFC membranes through simultaneous one-step sol–gel reaction and reactive extrusion. *Mater. Chem. Phys.* **2015**, *163*, 54–62. [CrossRef]
21. Velikova, N.; Spassova, I. Bifunctional mesoporous hybrid sol-gel prepared silicas for CO_2 adsorption. *J. Sol-Gel Sci. Technol.* **2021**, *100*, 326–340. [CrossRef]
22. Wan, H.; Mills, R.; Qu, K.; Hower, J.C.; Mottaleb, M.A.; Bhattacharyya, D.; Xu, Z. Rapid removal of PFOA and PFOS via modified industrial solid waste: Mechanisms and influences of water matrices. *Chem. Eng. J.* **2022**, *433*, 133271. [CrossRef]
23. Guo, C.; Ding, H.; Xie, M.; Zhang, H.; Hong, X.; Sun, L.; Ding, F. Multifunctional superamphiphobic fluorinated silica with a core-shell structure for anti-fouling and anti-corrosion applications. *Colloids Surf. A Physicochem. Eng. Asp.* **2021**, *615*, 126155. [CrossRef]
24. Yu, F.; Gao, J.; Liu, C.; Chen, Y.; Zhong, G.; Hodges, C.; Chen, M.; Zhang, H. Preparation and UV aging of nano-SiO_2/fluorinated polyacrylate polyurethane hydrophobic composite coating. *Prog. Org. Coatings* **2020**, *141*, 105556. [CrossRef]
25. Startek, K.; Arabasz, S.; Bachmatiuk, A.; Lukowiak, A. Influence of fluoroalkyl chains on structural, morphological, and optical properties of silica-based coatings on flexible substrate. *Opt. Mater.* **2021**, *121*, 111524. [CrossRef]
26. Banerjee, D.A.; Kessman, A.J.; Cairns, D.R.; Sierros, K.A. Tribology of silica nanoparticle-reinforced, hydrophobic sol–gel composite coatings. *Surf. Coatings Technol.* **2014**, *260*, 214–219. [CrossRef]
27. Li, Q.; Yan, Y.; Yu, M.; Song, B.; Shi, S.; Gong, Y. Synthesis of polymeric fluorinated sol–gel precursor for fabrication of superhydrophobic coating. *Appl. Surf. Sci.* **2016**, *367*, 101–108. [CrossRef]
28. Huang, C.-M.; Wang, H.-Y.; Fang, S.-Y.; Yang, W.-D. Influence of Fluorine-Containing Monomer Content on the Hydrophobic and Transparent Properties of Nanohybrid Silica Polyacrylate Coating Materials. *Materials* **2021**, *14*, 4261. [CrossRef]
29. Nimittrakoolchai, O.-U.; Supothina, S. Preparation of stable ultrahydrophobic and superoleophobic silica-based coating. *J. Nanosci. Nanotechnol.* **2012**, *12*, 4962–4968. [CrossRef]
30. Shao, J.; Zhao, Y.; Li, D.; Xu, S.; Dou, Z.; Sun, Z.; Cao, M.; Fu, K.; Liu, Y.; Zhou, Y. Synthesis and characterization of superhydrophobic fluorinated mesoporous silica for oil/water separation. *Microporous Mesoporous Mater.* **2022**, *344*, 112240. [CrossRef]
31. El Fouhaili, B.; Ibrahim, A.; Dietlin, C.; Chemtob, A.; Allonas, X.; Croutxé-Barghorn, C. Single-step formation of superhydrophobic surfaces using photobase-catalyzed sol-gel process. *Prog. Org. Coatings* **2019**, *137*, 105293. [CrossRef]
32. Saboori, R.; Azin, R.; Osfouri, S.; Sabbaghi, S.; Bahramian, A. Synthesis of fluorine- doped silica-coating by fluorosilane nanofluid to ultrahydrophobic and ultraoleophobic surface. *Mater. Res. Express* **2017**, *4*, 105010. [CrossRef]
33. Li, K.-M.; Jiang, J.-G.; Tian, S.-C.; Chen, X.-J.; Yan, F. Influence of Silica Types on Synthesis and Performance of Amine–Silica Hybrid Materials Used for CO_2 Capture. *J. Phys. Chem. C* **2014**, *118*, 2454–2462. [CrossRef]
34. Waseem, M.; Mustafa, S.; Naeem, A.; Shah, K.H.; Shah, I.; Ihsan-ul-Haque. Synthesis and characterization of silica by sol-gel method. *J. Pak. Mater. Soc.* **2009**, *3*, 19–21. Available online: https://www.researchgate.net/publication/285105909 (accessed on 10 November 2022).

35. Cai, S.; Zhang, Y.L.; Zhang, H.L.; Yan, H.W.; Lv, H.B.; Jiang, B. Sol–Gel Preparation of Hydrophobic Silica Antireflective Coatings with Low Refractive Index by Base/Acid Two-Step Catalysis. *ACS Appl. Mater. Interfaces* **2014**, *6*, 11470–11475. [CrossRef]
36. Yu, Q.; Xu, J. Structure and surface properties of fluorinated organic–inorganic hybrid films. *J. Sol-Gel Sci. Technol.* **2012**, *61*, 243–248. [CrossRef]
37. Wagh, P.B.; Kumar, R.; Patel, R.P.; Singh, I.K.; Ingale, S.V.; Gupta, S.C.; Mahadik, D.B.; Venkateswara Rao, A. Hydrophobicity measurement studies of silica aerogels using ftir spectroscopy, weight difference method, contact angle method and k-f titration method. *J. Chem. Bio. Phys. Sci. Sec. A* **2015**, *5*, 2350–2359.
38. Ni, H.; Wang, X.; Zhang, W.; Wang, X.; Shen, Z. Stable hydrophobic surfaces created by self-assembly of poly(methyl methacrylate) end-capped with 2-perfluorooctylethyl methacrylate units. *Surf. Sci.* **2007**, *601*, 3632–3639. [CrossRef]
39. Yao, L.; Yang, T.; Cheng, S. Synthesis and characterization of poly(fluorinated acrylate)/silica hybrid nanocomposites. *J. Appl. Polym. Sci.* **2010**, *115*, 3500–3507. [CrossRef]
40. Fang, C.; Huang, X.; Ge, T.; Li, Y.; Cao, Y.; Zhu, X.; Dong, X. Effect of dodecafluoroheptyl methacrylate (DFMA) on the comprehensive properties of acrylate emulsion pressure sensitive adhesives. *Int. J. Adhes. Adhes.* **2020**, *101*, 102634. [CrossRef]
41. Spataru, C.I.; Purcar, V.; Ghiurea, M.; Radovici, C.; Stanga, G.; Donescu, D. Effects of the nanoassociation of hexadecyltrimethoxysilane precursors on the sol–gel process. *J. Sol-Gel Sci. Technol.* **2013**, *65*, 344–352. [CrossRef]
42. Petcu, C.; Purcar, V.; Ianchiş, R.; Spătaru, C.-I.; Ghiurea, M.; Nicolae, C.A.; Stroescu, H.; Atanase, L.-I.; Frone, A.N.; Trică, B.; et al. Synthesis and characterization of polymer-silica hybrid latexes and sol-gel-derived films. *Appl. Surf. Sci.* **2016**, *389*, 666–672. [CrossRef]
43. Zhou, G.; Simerly, T.; Golovko, L.; Tychinin, I.; Trachevsky, V.; Gomza, Y.; Vasiliev, A. Highly functionalized bridged silsesquioxanes. *J. Sol-Gel Sci. Technol.* **2012**, *62*, 470–482. [CrossRef]
44. Campostrini, R.; Ischia, M.; Carturan, G.; Gialanella, S.; Armelao, L. Rh Inclusion in Sol-Gel SiO2. Effects of Rh Precursors on Metal Dispersion and SiO_2-Rh Thermal Behavior. *J. Sol-Gel Sci. Technol.* **2000**, *18*, 61–76. [CrossRef]
45. da Silva, D.G.; Costa, V.C.; Nunes, R.A.X. Preparation of Antireflective Silica Coating by the Sol-Gel Method for Heliothermic Power Plants. *Mater. Res.* **2018**, *21*, e20170970. [CrossRef]
46. Huang, X.; Liao, W.; Ye, L.; Zhang, N.; Lan, S.; Fan, H.; Qu, J. Fabrication of hydrophobic composite films by sol-gel process between POSS -containing fluorinated polyacrylate latexes and colloidal silica particles. *Microporous Mesoporous Mater.* **2017**, *243*, 311–318. [CrossRef]
47. Tadjarodi, A.; Haghverdi, M.; Mohammadi, V.; Rajabi, M. Synthesis and characterization of hydrophobic silica aerogel by two 411 step (acid-base) sol-gel process. *J. Nanostruct.* **2013**, *3*, 181–189. [CrossRef]
48. Tao, C.; Yan, H.; Yuan, X.; Yin, Q.; Zhu, J.; Ni, W.; Yan, L.; Zhang, L. Sol-gel based antireflective coatings with superhydrophobicity and exceptionally low refractive indices built from trimethylsilanized hollow silica nanoparticles. *Colloids Surf. A Physicochem. Eng. Asp.* **2016**, *509*, 307–313. [CrossRef]
49. Capeletti, B.L.; Zimnoch, J.H. Fourier Transform Infrared and Raman Characterization of Silica-Based Materials. In *Applications of 416 Molecular Spectroscopy to Current Research in the Chemical and Biological Sciences*; Mark, T.S., Ed.; IntechOpen: London, UK, 2016; pp. 1–21.
50. El-Denglawey, A.; Makhlouf, M.; Dongol, M. The effect of thickness on the structural and optical properties of nano Ge-Te-Cu films. *Results Phys.* **2018**, *10*, 714–720. [CrossRef]
51. Borkar, S.; Jankova, K.; Siesler, H.W.; Hvilsted, S. New Highly Fluorinated Styrene-Based Materials with Low Surface Energy Prepared by ATRP. *Macromolecules* **2004**, *37*, 788–794. [CrossRef]
52. Zhang, Q.; Zhan, X.; Chen, F.; Shi, Y.; Wang, Q. Block copolymers of dodecafluoroheptyl methacrylate and butyl methacrylate by RAFT miniemulsion polymerization. *J. Polym. Sci. Part A Polym. Chem.* **2007**, *45*, 1585–1594. [CrossRef]
53. Brassard, J.-D.; Sarkar, D.K.; Perron, J. Synthesis of Monodisperse Fluorinated Silica Nanoparticles and Their Superhydrophobic Thin Films. *ACS Appl. Mater. Interfaces* **2011**, *3*, 3583–3588. [CrossRef]